Environ Geol
DOI 10.1007/s00254-008-1234-z

ORIGINAL ARTICLE

Mobilization of Ag, heavy metals and Eu from the waste deposit of the Las Herrerias mine (Almería, SE Spain)

A. Navarro · E. Cardellach

Received: 7 September 2007 / Accepted: 3 February 2008

Abstract We studied the mobility of silver, heavy metals and europium in waste from the Las Herrerías mine in Almería (SE Spain). The most abundant primary mineral phases in the mine wastes are hematite, hydrohematite, barite, quartz, muscovite, anorthite, calcite and phillipsite. The minor phase consisted of primary minerals including ankerite, cinnabar, digenite, magnesite, stannite, siderite and jamesonite, and secondary minerals such as glauberite, szomolnokite, thenardite and uklonscovite. The soils show high concentrations of Ag (mean 21.6 mg kg^{-1}), Ba (mean 2.5%), Fe (mean 114,000 mg kg^{-1}), Sb (mean 342.5 mg kg^{-1}), Pb (mean 1,229.8 mg kg^{-1}), Zn (mean 493 mg kg^{-1}), Mn (mean 4,321.1 mg kg^{-1}), Cd (mean 1.2 mg kg^{-1}) and Eu (mean 4.0 mg kg^{-1}). The column experiments showed mobilization of Ag, Al, Ba, Cu, Cd, Eu, Fe, Mn, Ni, Sb, Pb and Zn, and the inverse modelling showed that the dissolution of hematite, hausmannite, pyrolusite and anglesite can largely account for the mobilization of Fe, Mn and Pb in the leaching experiment. The mobility of silver may be caused by the presence of kongsbergite and chlorargyrite in the waste, while the mobility of Eu seems to be determined by $Eu(OH)_3$, which controls the solubility of Eu in the pH–Eh conditions of the experiments. The mineralogy, pH, Eh and geochemical composition of the mine wastes may explain the possible mobilization of heavy metals and metalloids. However, the absence of contaminants in the groundwater may be caused by the carbonate-rich environment of "host-rocks" that limits their mobility.

Keywords Mine wastes · Ag · Heavy metals · Leaching · Mineral phase

A. Navarro (✉)
Depto. M. Fluidos, ETSEIT,
Universidad Politécnica de Cataluña,
Colón 7, 08222 Terrassa, Spain
e-mail: navarro@mf.upc.edu

E. Cardellach
Dep. Geologia, Universitat Autónoma de Barcelona,
08193 Bellaterra, Spain

Introduction

There are hundreds of abandoned mining sites in southeast Spain, especially in the ancient mining districts of Las Herrerías and Sierra Almagrera, located in the NE of Almería province in Andalucía (Fig. 1a), most of which were active between 1838 and 1991. Most of these sites are contaminated and have an environmental impact on soils, aquifers, surface waters and coastal marine waters in some areas (Navarro et al. 2000, 2004, 2006; Robles-Arenas et al. 2006; Wray 1998).

The abandoned mine waste associated with sulfide mining is often a major source of metal pollutants in watercourses and soils and causes the degradation of local ecosystems (Lottermoser 2003).

When pyrite (FeS_2) and other sulfide minerals are exposed to atmospheric oxygen and moisture, they undergo a series of weathering reactions that release large amounts of As, Cd, Cu, Co, Cr, Fe, Mo, Ni, Pb, Sb, Zn and other minor elements (EPA 1996; Herbert 1996; Stollenwerk 1994; Blowes and Ptacek 1994; Dold and Fontboté 2001, 2002; Blowes et al. 2003; Romero et al. 2006, 2007) into the soil and/or groundwater, in a low-pH medium produced by sulfide oxidation. When the system is capable of neutralizing the pH, the high concentrations of dissolved metals are attenuated by a series of precipitation, coprecipitation and adsorption reactions related to the formation

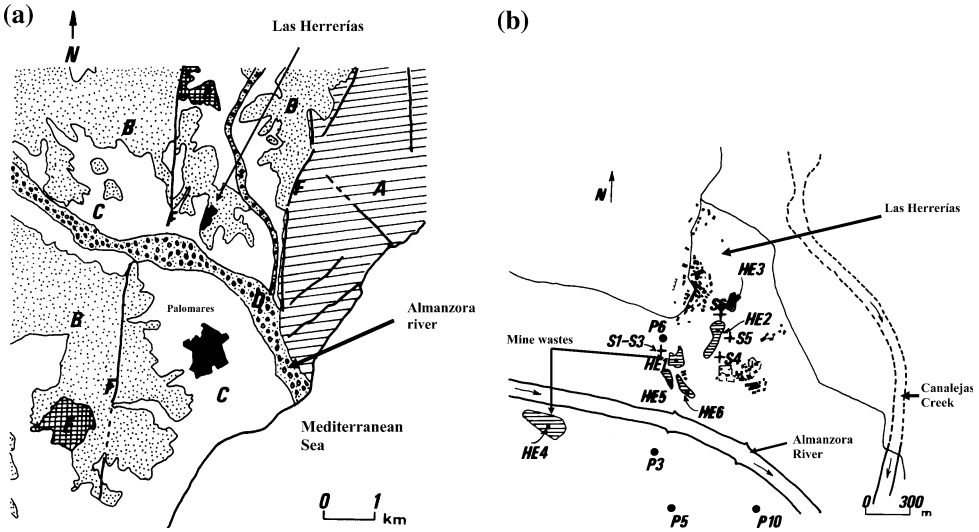

Fig. 1 **a** Location map of the Las Herrerías study area. *a* Nevado–Filabride complex (metamorphic basement), *b* tertiary (Tortonian–Pliocene) sediments (marls, silty marls and marly clays), *c* Pleistocene–Holocene (old fluvial terraces), *d* Holocene (recent fluvial terraces), *e* tertiary shoshonitic volcanics and *f* main fractures. **b** Location map of the sampled wells, soils and mine waste used in the lixiviation tests. *HE* mine waste and *S* soils, *HE1–HE3* mine waste samples used in the lixiviation tests

of secondary phases, which include water-soluble sulfates such as efflorescent salts.

The precipitation of secondary sulfates and oxyhydroxide phases in the non-saturated zone of contaminated areas sometimes produces precipitate layers known as "hard-pans", which control the movement of O_2 and dissolved metals through mine waste and soil and which have significant environmental implications (Blowes and Jambor 1990; McGregor et al. 1998; Ribet et al. 1995; Al et al. 2000).

The precipitation of secondary minerals may also control pore-water acidity and the distribution of trace elements. In semi-arid regions like the study area in this case (Fig. 1a), the dissolution of most soluble metal-sulfate secondary phases following storm runoff events can mobilize the contaminants, which increases the concentration of dissolved metals and sulfates in streams, groundwater and leachates from tailings and mine waste (Jambor et al. 2000; Dold and Fontboté 2001; Buckby et al. 2003; Lottermoser 2003; Ptacek and Blowes 2003; Navarro et al. 2004; Ashley et al. 2004; Blowes et al. 2004).

As a consequence, the oxidation of sulfides and sulfosalts in the nearby Sierra Almagrera led to the precipitation of secondary phases, such as jarosite [$KFe_3(SO_4)_2(OH)_6$], natrojarosite [$NaFe_3(SO_4)_2(OH)_6$], crystalline Fe-oxyhydroxide (goethite), amorphous ferric hydroxide [$Fe(OH)_3$], clay minerals, anglesite ($PbSO_4$), alunite [$KAl_3(SO_4)_2(OH)_6$], gypsum ($CaSO_4{\cdot}2H_2O$) and other minor phases (Navarro et al. 2000, 2004).

Barite sedimentary-exhalative deposits commonly form almost monomineralic layers with coarse-grained crustiform textures in the vein structures, which can be interpreted as feeder hydrothermal areas. These deposits may be several hundred meters or even several kilometers wide and have a proximal zone to a feeder hydrothermal area containing stratiform sulfide minerals such as chalcopyrite-pyrrhotite, sphalerite-galena and pyrite.

The presence of iron-rich zones in other deposits can create an acidic environment and the formation of secondary lead–manganese minerals and secondary sulfates of iron, aluminium and potassium. These may dissolve during periodic storms, which can mobilize the metals and lead to the emission of pulses of acidic waters into the environment. The secondary minerals in these deposits are goethite, hematite, with minor kaolinite and beudantite, with lead minerals such as anglesite and cerussite and secondary sulfate minerals including jarosite, barite and alunite (Kelley et al. 1996).

These deposits may have a high mercury content due to the close association of mercury with sphalerite in zinc-rich ores (Rytuba 2003), the amounts may range between 27 and 1,198 mg kg^{-1} Hg (Schwartz 1997). In sedex deposits, the dominant mercury phases are Hg solid solution in sphalerite (ZnS) and occasionally, cinnabar.

The drainage signatures of these deposits in poor-carbonate areas are low pH stream waters (2.8–4.7) and abundant dissolved metal, from tens to hundreds of mg L^{-1} of Al and Fe, and very large amounts of Mn, Cd, Co, Cu, Ni, Pb and Zn (Kelley et al. 1996). The most abundant soil and sediment contaminants in the areas surrounding these mining areas are Ag, As, Cd, Hg, Sb, Cu, Ni, Mn, Pb, Zn and Ba.

The aims of this study were to evaluate the mobility of silver, some heavy metals, metalloids and europium from the mine wastes of Las Herrerías mine and to identify the solid-phase that controls the mobility of these contaminants.

Study area

Location, geology and mineral deposits

The mining district of Las Herrerías is situated close to the Sierra Almagrera (SA) (Fig. 1a), which is located 90 km to

the northeast of Almería (SE Spain). It is one of the oldest metallurgical and mining areas in the Iberian Peninsula, together with the Iberian Pyrite Belt and the Cartagena mining district (Navarro et al. 2004).

The Las Herrerías mining area is part of the inner Betic Cordillera range (Fig. 1a). The host rocks of the Herrerías deposit are Upper Miocene marine sediments from the Neogene neotectonic basin of Vera-Garrucha.

The mineralization in Las Herrerías essentially consists of Fe-oxides, layers of barite, chert, native silver and some base metal sulfides in particular areas (galena, sphalerite, pyrite). These minerals form part of beds of mineralized exhalites, veins and pipes, Fe-oxide crusts and dissemination areas (López et al. 1993).

The stratigraphic sequence is as follows:

1. Metamorphic basement.
2. Mineralized marls and silty marls with Fe-oxides and barite.
3. Black iron oxides and barite veins.
4. Laminated barite and chert.
5. Exhalite deposits (sheet-like siliceous deposits).
6. Green marly clays (Messinian).

Martínez et al. (1992) suggested that the nature of the deposits in this area may be due to a combined submarine epithermal and hydrothermal origin during the upper miocene, since they are spatially and temporarily associated with shoshonitic volcanism.

The Las Herrerías deposit is predominantly an iron–barite–silver deposit that has similar characteristics to classic sedimentary-exhalative deposits. Although the deposit shows uniform characteristics, the exploited ore bodies may be the result of the uptake of hydrothermal fluids along the Las Herrerías fault structures (Booth-Rea et al. 2003).

Mining in the study area began in the 19th Century with the extraction of the Pb–Zn sulfides, which were exhausted before the last period of exploitation (1991–2005).

It is also interesting to note the large amount of silver contained by the mined ore in bonanza deposits in laminated barite and upper jasper. This led to the intensive exploitation of the ore deposit during the period 1871–1886, when a total of 600 tone of Ag-metal was produced, mainly from possible silver sulfides and kongsbergite.

Methodology

Mineralization, wastes, soil sampling and analysis

The mineralization, mine wastes and soils were manually extracted, with samples of, approximately, 1.5 kg obtained. These comprised 15 samples of outcroping mineralization, 6 samples of mine wastes and 6 samples of soils (Fig. 1b). The sampling strategy was aimed at obtaining representative samples of a complex mineralization and disseminated waste deposits. Black iron oxides, laminated layers of barite and cherts, barite veins filling open fissures in the stratigraphic sequence and barite lenses into the messinian marly clays were therefore sampled. The mine wastes are deposited around the main mining works (Fig. 1b), in small accumulations, with the six most representative deposits and six soils located near these waste deposits being sampled.

Old tailings and stockpiles are spread throughout the non-confined aquifer formed by the alluvial and deltaic deposits of the Almanzora River close to the old mining facilities. The area is currently used intensively for agriculture.

Outcropping mineralization (15 samples), waste (6 samples) and soil samples (6 samples) from 27 locations were crushed to 10 mesh in a jaw crusher, quartered, pulverized in an agate mortar, rehomogenized and repacked in plastic bags. Soil samples were taken from a depth of approximately, 0–0.25 m and were sent to Actlabs (Ontario, Canada) with the other samples. Au, Ag, As, Ba, Br, Ca, Ce, Co, Cr, Cs, Eu, Fe, Hf, Hg, Ir, La, Lu, Na, Ni, Nd, Rb, Sb, Sc, Se, Sm, Sn, Sr, Ta, Th, Tb, U, W, Y and Yb were quantitatively analyzed by instrumental neutron activation analysis (INAA) and Mo, Cu, Pb, Zn, Ag, Ni, Mn, Sr, Cd, Bi, V, Ca, P, Mg, Tl, Al, K, Y and Be were analyzed by inductively coupled plasma emission spectroscopy (ICP-OES).

Mine waste samples were studied using transmitted and reflected light microscopy, X-ray diffraction (XRD) and scanning electron microscopy (SEM) with an attached energy dispersive system (EDAX) and with an electron microprobe (EMPA). These techniques enabled us to identify the mineral phases and to analyze the major and trace element contents of the most abundant minerals.

Groundwater sampling and analysis

Samples of groundwater (P-6, P-3, P-5 and P-10) used for agricultural proposes were obtained in wells located close to the mining area at a depth of approximately 36 m (Fig. 1b). In situ parameters, such as pH, redox potential (Eh, mV) and electrical conductivity (EC, $\mu S\ cm^{-1}$) were measured with portable devices, which were calibrated by standard solutions.

Water samples for chemical analyses were filtered through a 0.45 μm pore-size cellulose nitrate membrane filter. Samples for cation analyses were acidified to pH $<$ 2.0 by adding a few drops of 50% ultrapure HNO_3. Each water sample was transferred to the laboratories in high-

density 500 ml polypropylene bottles, which were tightly sealed with a double cap and stored in a refrigerator prior to analysis.

Major dissolved ionic constituents and trace elements in the samples were analyzed in laboratories at the University of Barcelona. Metal concentrations were determined with acidified (HNO_3) samples by using inductively coupled plasma atomic emission spectroscopy (ICP-AES) for major elements (Na, Ca, Mg, K, Sr, S, Si, Fe and P) and a mass detector (ICP-MS) for minor elements (Mn, Al, Ba, Zn, Li, Pb, Rb, Cu, U, Sb, Sn, Cd, Mo, Hg, Se, Cr, As, Ni and Co). The concentrations of chloride, nitrate and sulfate in a second, untreated sample were analyzed by ion chromatography and the alkalinity of the waters was analyzed by titration.

Column experiments

We conducted laboratory column experiments to simulate the mobilization of contaminants from mine waste in similar conditions to those present in the study area.

The column used in this study was 751 mm long with an internal diameter of 150 mm and an endpiece fitted with a 0.50 μm filter. Leaching was induced by pumping low-mineral water into the column using a "rain-simulator" connected to a titration pump that provided a maximum flow rate of 10 L h^{-1}. Three mine waste samples were subjected to leaching at a stationary flow rate of 3.44 L h^{-1} until a "pore volume" of 28.4 was obtained. The "pore volume", or dimensional time, is the leached pore volume of flow at the end of the column, which is defined as follows:

$$T' = v\,t/L \quad (1)$$

where v is the average linear fluid velocity (pore velocity), t is the elapsed time and L is the length of the column. The samples were collected at the bottom of the column as a function of time. The first sample, corresponding to time 0, was taken when the water started to flow from the bottom of the column and the flow-rate, pH, Eh and conductivity were measured immediately after collection of the sample. The leachates were obtained from three solid wastes: HE1 (old mining wastes which were deposited between 1871 and 1886), HE2 (barite spoils generated between 1991 and 2005) and HE3 (mine wastes impoundments from the deeper levels of the exploitation generated between 2001 and 2005), whose geochemical composition is shown in Table 1.

The effluents obtained from the experiments were filtered using cellulose nitrate films with a diameter of 0.45 μm and stored at 4°C. Effluent pH, temperature, oxidation–reduction potential and electrical conductivity were determined beforehand. The pH was measured potentiometrically and the pH meter was calibrated before testing each sample. Conductivity was determined using a conductimeter calibrated with NaCl for each effluent sample.

Table 1 Geochemical composition of the waste samples used in the leaching test

Element	HE1	HE2	HE3
Au	10	15	<2
Ag	3.5	41.2	32.8
Cu	172	23	62
Cd	1.3	0.6	2.5
Mo	8	4	9
Pb	2,880	887	1,560
Ni	22	5	42
Zn	780	369	1,430
S	0.4	0.29	0.42
Al	0.48	0.11	1.08
As	101	29.9	62.3
Ba	176,000	437,000	69,300
Co	8	<1	8
Cr	22	28	74
Eu	25.4	10.4	6.5
Fe	23.4	3.97	24.3
Hg	<1	12	<1
Mn	5,340	387	15,900
Sb	1,170	540	1,210
Se	<3	<3	<3
W	33	34	8

HE1 old mining wastes, *HE2* barite spoils from present mining activities, *HE3* present mining wastes and deep host-rock

Values are in mg kg^{-1}, except Al, S and Fe (%) and Au (μg kg^{-1})

The oxidation–reduction potential was measured using an ORP meter with a combined platinum electrode. The lixiviates were analyzed to determine the main cations, metals and rare elements in acidified (ultrapure HNO_3) samples with a maximum acidity of pH 1.5 using inductively coupled plasma atomic emission spectroscopy (ICP-OES). The concentrations of chloride, nitrate, nitrite, fluoride, bromide, phosphate and sulfate in a second untreated sample were analyzed by ion chromatography.

Results

Mine wastes

Mine wastes from the Las Herrerías area are a result of ore milling in the 19th century (mainly sulfide-rich ore and silver mineralization) and the treatment of ore using gravitational methods. There are also more recent mine wastes that include tailings formed during barite concentration

by dense medium separation and the overburden and host-rock of the deeper mineralization (mined during the most recent period of exploitation: 2000–2003), which mainly consist of Fe oxides (Fig. 2).

The mineralization and waste sample results (Table 2) show similar range values for mineralization and waste samples, which contain high concentrations of Ag, As, Ba, Fe, Hg, Sb, Eu, Pb, Zn and Mn. However, the concentrations of certain metals were higher in the waste samples, possibly because the mineralization sample materials analyzed were found only in the outcropping deposits. In addition, the high concentrations of residual metals, such as Ag, Pb, Sb and Zn in the mine wastes are indicative of the low efficiency of ore processing in the 19th Century. The "old" wastes are composed of sand-silt crushed ore with brown coloration that has a similar composition to other Ag–Pb–Zn mine wastes (Ashley et al. 2004; Navarro et al. 2004; Harris et al. 2003; Robles-Arenas et al. 2006).

The wastes show very diverse mineralogies, which consist of a dominant species and minor phases (Table 3). The most abundant primary mineral phases are hematite, hydrohematite, barite, quartz, muscovite, anorthite, calcite and phillipsite. The minor phase minerals (Table 3) are primary minerals, such as aikinite, ankerite, canfieldite, cattierite, cinnabar, digenite, empresite, jamesonite, kongsbergite, magnesite, siderite, smithite, stannite and violarite; and secondary minerals, such as emmoncite, glauberite, halite, hausmannite, macedonite, senarmontite, szomolnokite, thenardite and uklonscovite. The presence of efflorescent salts such as szomolnokite and other sulfates, which dissolve during damp periods, may explain the mobilization of some contaminants. The dissolution of these phases releases Fe^{2+}, which raises acidity during dissolution and leads to the generation of lixiviates with high concentrations of Fe, Na and Mg. Hardpan formation was not detected, possibly due to the scarcity of sulfides, which leads to limited production of secondary mineral phases.

SEM observations revealed particles of silver minerals, such as acantite (Fig. 3), kongsbergite and chlorargyrite (Fig. 4). The presence of acantite may be associated with silver-sulfides, while kongsbergite and chlorargyrite are possible supergenic phase minerals and the focus of Ag detected in the leaching experiments.

Soils

Soil samples taken from the areas above and around the mine workings show high concentrations of Ag (mean 21.6 mg kg^{-1}), Ba (mean 2.5%), Fe (mean 114,000 mg kg^{-1}), Sb (mean 342.5 mg kg^{-1}), Pb (mean 1,229.8 mg kg^{-1}), Zn (mean 493 mg kg^{-1}), Mn (mean 4,321.1 mg kg^{-1}), Cd (mean 1.2 mg kg^{-1}) and Eu (mean 4.0 mg kg^{-1}). The metal content of the sampled soils (Table 2) were 1–2 orders of magnitude higher than the alluvial "non-contaminated" soils (Table 2), except for Fe and Eu, which show minor enrichment.

The metal enrichment could reflect the mechanical dispersion of contaminants from mine wastes and mining works caused by the transportation of dust particles in

Fig. 2 **a** View of current barite ore stockpiles and the waste rock spoils in Las Herrerías, **b** view of the last open pit exploitation showing the overburden (light materials) of Messinian marly clays and the mineralization at depth, **c** current mine wastes and abandoned mining facilities and **d** view of current mine wastes, mainly composed of hematite, hydrohematite, barite and quartz

Table 2 Concentrations of metals and metalloids in mineralization, mine waste and soils in Las Herrerías (Almería)

	Au	Ag	As	Ba	Co	Cr	Fe	Hg	Ni	Sb	Se	W	Eu	Cu	Pb	Zn	Mn	Cd
Mineralization ($n = 15$)																		
Mean	14.6	22.5	49.8	28.9	6.7	65.1	9.2	4.9	92.6	364.8	5.9	22.7	10.7	20.5	519	574.9	205	0.6
Median	9.0	10.0	18.0	39.0	5.0	29.0	4.0	3.0	50.0	180	5.0	4.0	10.4	20.5	519	234	205	0.6
Minimum	4.0	5.0	2.0	0.05	1.0	10.0	0.6	1.0	5.0	4.6	3.0	1.0	0.8	18.0	151	70	23	0.5
Maximum	44.0	150.0	340.0	49.0	28.0	370.0	35.4	18.0	570.0	1,600	19.0	150	36.0	23.0	887	3,320	387	0.6
Std. dev.	13.3	37.3	86.8	19.3	6.5	92.3	12.1	5.1	135.4	483.5	3.8	43.3	9.9	3.5	520.4	917.2	254.7	0.1
Mine waste ($n = 6$)																		
Mean	17.5	28.4	79.7	20.2	5.5	30.2	21.2	2.8	29.8	1,090	3.7	19.2	14.3	72.8	1,561.5	979.2	5,578	1.3
Median	14.0	30.9	87.5	13.8	6.5	25.0	23.9	1.0	33.5	1,185	3.0	20.5	12.3	48.0	1,239.5	1020	3,012.5	1.1
Minimum	2.0	3.5	29.9	6.9	1.0	10.0	3.97	1.0	2.0	540	3.0	1.0	6.5	23.0	887	356	387	0.6
Maximum	45.0	47.0	110.0	43.7	8.0	74.0	33.7	12.0	53.0	1,320	5.0	35.0	25.4	172.0	2,880	1680	15,900	2.5
Std. dev.	14.9	16.0	29.5	15.8	2.9	22.9	11.0	4.5	23.3	278.7	1.0	16.4	6.8	68.2	932.1	561	7,245.4	0.8
Soils ($n = 6$)																		
Mean	5.0	21.6	27.8	2.5	9.8	58.0	11.4	<1	25.0	342.5	4.0	2.6	4.0	31.5	1,229.8	493	4,321.1	1.2
Median	5.0	21.5	27.0	1.5	9.0	53.0	10.7	–	26.0	300	4.0	2.5	3.9	32.5	1,313.5	486	4,372	1.4
Minimum	2.0	5.0	4.0	0.05	5.0	40.0	2.0	–	14.0	12	3.0	1.0	1.0	12	33	66.0	308	0.5
Maximum	10.0	46.0	65.0	8.6	14.0	98.0	26.1	–	34.0	1,000	5.0	5.0	8.6	54	2,453	1247	8,270	2.1
Std. dev.	2.9	2.9	21.2	3.0	3.2	21.5	8.8	–	6.9	364.9	1.1	1.8	2.6	15.1	1,150.4	437.9	3,362.2	0.6
NCD (mean)	3.7	<0.4	12.2	0.03	12.5	–	3.7	<1	20	83.4	<3	3	1.2	19.2	21.2	74.7	369.2	<0.5
NIL	–	–	55	0.062	240	380	–	10	210	–	–	–	–	190	530	720	–	12

Values are in mg kg^{-1} except Ba and Fe (%) and Au (μg kg^{-1})

NIL The Netherlands soil intervention values, *NCD* non-contaminated soils, sampled in alluvial sediments upstream from the mining area

semi-arid environments. It could also be an evidence of reactive–dispersive phenomena caused by the weathering of primary minerals and the subsequent transportation of contaminants in water during damp periods.

Comparison of the mean soil concentrations and The Netherlands soil intervention values (one of the most commonly used quality levels in soil analysis) shows that only Ba and Pb concentrations were above the intervention values. However, we also recorded high concentrations of other elements that are not included in these soil regulations, such as Ag, Sb and Mn.

The soil samples are mineralogically complex (Table 4) and consist of primary phases, such as barite, stibnite and proustite; low-solubility secondary phases, such as cerusite, zincosite, gibbsite and mimetesite; and low-solubility sulfate minerals, such as anglesite, argentojarosite, celestite, brochantite, fibroferrite, langite and uklonscovite, in addition to other less-frequently occurring minerals. We also detected medium/high-solubility sulfate minerals, such as bianchite, bieberite, gunningite, kieserite, szmikite, szomolnokite, apjohnite and halotrichite.

Groundwater

Groundwater samples (P-6, P-3, P-5 and P-10) were collected downstream of the mining area. The results show a progressive decrease in electrical conductivity between the sampling-point located close to Las Herrerías (P-6) and the well furthest away (P-10) (Table 5). In addition, the levels of B, Sr, Si, Li, Zn, Na, Ca and Mg decrease as the groundwater flows away from the potential focus of contamination, which should reflect the attenuation of contaminants in the saturated zone of the aquifer. There is also considerable attenuation in the non-saturated zone, since the concentrations of heavy-metals detected are very low.

There is no clear evolution of other contaminants, such as Ba, Pb, Mn and Fe and the detected levels seem to be stabilized. Only B (P-6), Na (P-3, P-5, P-6 and P-10) and Fe (P-5) exceed the maximum permitted levels established in the European drinking water standards (Table 5).

Leaching tests

The leaching results for samples HE1, HE2 and HE3 (Table 1) show mobilization of Ag, Al, Ba, Cu, Cd, Eu, Fe, Mn, Ni, Sb, Pb and Zn (Table 6). Al reaches concentrations of 1.5 mg L^{-1} in the HE1 leaching, 0.3 mg L^{-1} in the HE2 leaching and 5.1 mg L^{-1} in the HE3 leaching. Similarly, Fe and Mn concentrations are highest in the HE3 leaching, where they reach values of 1.8 and 4.2 mg L^{-1},

Table 3 Identified phase minerals in Las Herrerías mine wastes

Mineral phases	Formula
Primary phase	
Hematite[a]	Fe_2O_3
Hydrohematite[a]	$Fe_2O_3 \cdot H_2O$
Barite[a]	$BaSO_4$
Quartz[a]	SiO_2
Muscovite[a]	$Al_{2.9}H_2KO_{12}Si_{3.1}$
Anorthite[a]	$Ca(Al_2Si_2O_8)$
Calcite[a]	$CaCO_3$
Phillipsite	$K_2Ca_2(Al, Si)_{16}O_{32} \cdot 5\ H_2O$
Aikinite	$PbCuBiS_3$
Ankerite	$Ca(Fe, Mg, Mn)(CO_3)_2$
Canfieldite	Ag_8SnS_6
Cattierite	CoS_2
Cinnabar	HgS
Digenite	Cu_9S_5
Empresite	AgTe
Jamesonite	$Pb_4FeSb_6S_{14}$
Kongsbergite	Ag(Hg)
Magnesite	$MgCO_3$
Siderite	$FeCO_3$
Smithite	$AgAsS_2$
Stannite	Cu_2FeSn_4
Violarite	$FeNiS_4$
Secondary phase	
Emmoncite	$Fe_2Te_3O_9{\cdot}2H_2O$
Glauberite	$Na_2Ca(SO_4)_2$
Halite	NaCl
Hausmannite	$Mn^{2+}Mn_2^{3+}O_4$
Macedonite	$PbTiO_3$
Senarmontite	Sb_2O_3
Szomolnokite	$FeSO_4 \cdot H_2O$
Thenardite	$Na_2\ SO_4$
Uklonskovite	$NaMg(SO_4)F \cdot 2H_2O$

[a] Medium-abundance phase

respectively, and lowest in the HE2 leaching (<0.1 and 0.161 mg L^{-1}) and HE1 experiments (1.1 and 1.65 mg L^{-1}). Fe and Mn evolve differently in each leaching test, which suggests that the increased mobilization of Mn in the HE3 sample may be due to the fact that the concentration of the HE3 solid sample is higher (Fig. 5).

The highest concentration of Ba (Table 6) was recorded in the HE2 sample (0.33 mg L^{-1}), while the highest values of Cu, Pb, Sb and Eu were recorded in the HE1 leaching (0.073, 1.59, 0.022 and 0.008 mg L^{-1}, respectively). Ag, Cd and Zn showed similar figures and the highest concentrations were reached in the HE3 leaching (0.024, 0.003 and 0.51 mg L^{-1}, respectively). The HE3 sample showed the highest level of these metals, with the exception of Ag,

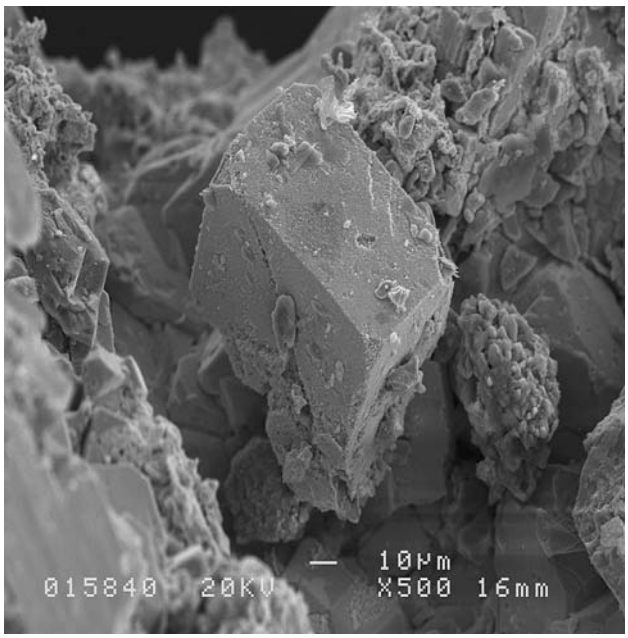

Fig. 3 Scanning electron photomicrographs of acantite over barite particles in the Las Herrerías mine wastes

the highest concentration of which was recorded in the HE2 sample.

The higher concentrations of Pb and Zn in the leaching (Figs. 6, 7) may reflect higher concentrations of these metals in the original sample before leaching. The leaching tests were also controlled for electrical conductivity, pH, Eh and O_2, which varied between the three samples throughout each 420-min assay. The results are for 28.4 pore volumes or water flow through the reactive material.

The pH was between 8.1 and 8.3 in all the samples and showed no clear evolution, which may indicate the presence of an alkaline medium that raises the pH. The Eh values were positive in all cases and ranged between 20 and 174 mV, the concentration of dissolved O_2 was almost 7.5 mg L^{-1} and electrical conductivity varied greatly between the three samples (Table 7).

In the HE1 sample (old mine wastes), the conductivity was therefore 4.5 mS cm^{-1} at the start of the leaching and 0.9 mS cm^{-1} at the end. The conductivity values in HE2 (present barite spoils) and HE3 (present mine wastes) were 4.7 and 0.8 mS cm^{-1}, respectively, at the start of the column experiment and 0.2 and 0.4 mS cm^{-1} at the end.

Geochemical modelling and mobilization of the main contaminants

Geochemical modelling

We used inverse modelling in the PHREEQC code to evaluate mass transfer in the column experiments

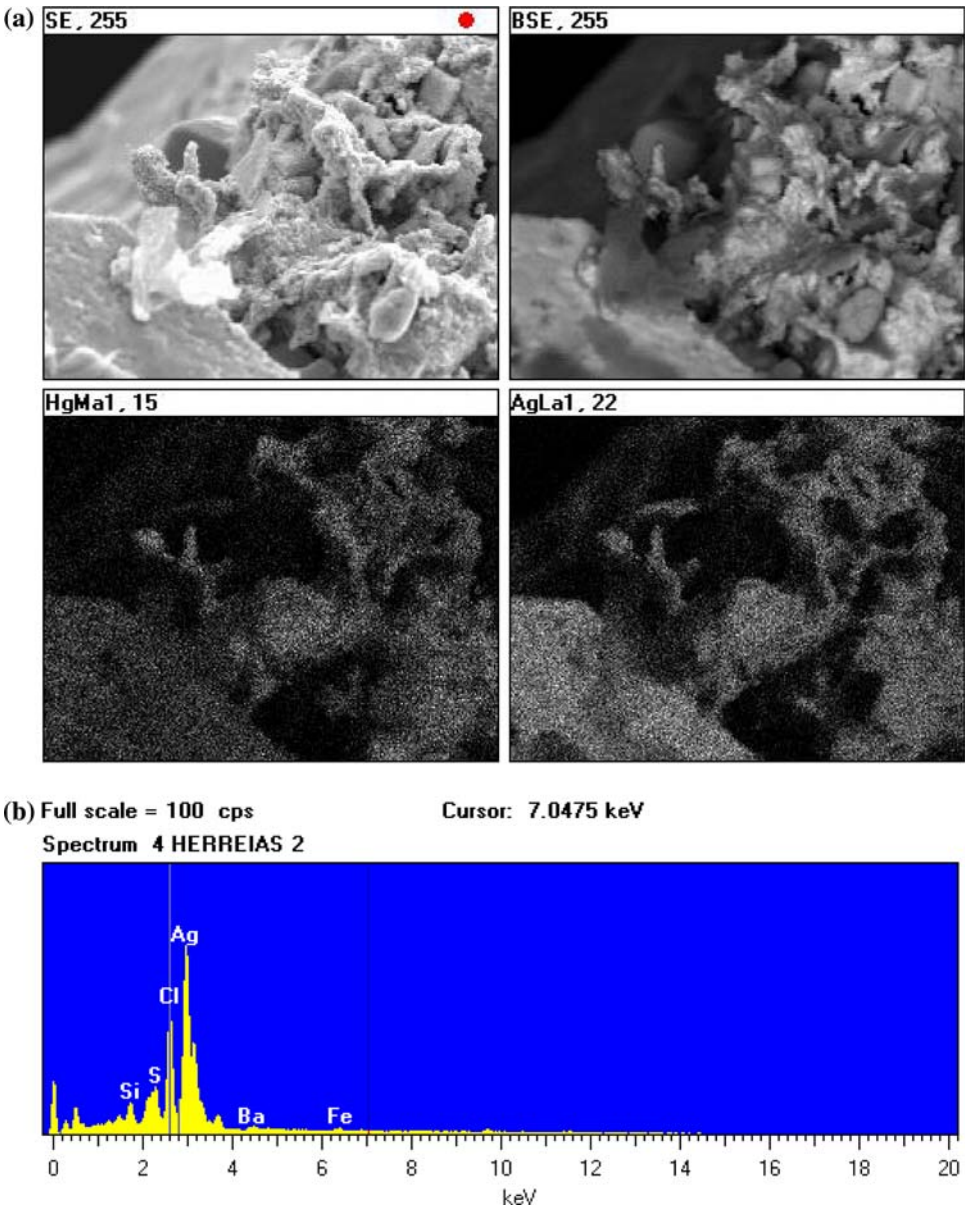

Fig. 4 **a** Scanning electron photomicrographs of kongsbergite and chlorargyrite and **b** XR spectra of chlorargyrite showing Ag and Cl dominant elements

(Parkhurst and Appelo 1999). Inverse modelling in the PHREEQC program is a geochemical mole-balance model that uses a set of defined minerals and on an optional basis, gases which are related to an entry solution and an output solution that account for the hydrogeochemical differences in the flow path. This numerical code in the "inverse modelling" form has previously been applied to environmental problems associated with mining (Armienta et al. 2001; Eary et al. 2003; Navarro et al. 2006) and in interpreting the geochemical properties of aquifers (Mahlknecht et al. 2004).

Hydrogeochemical analyses have been used to evaluate the speciation of dissolved constituents in leachates and to calculate the saturation state of the effluents with the numerical code PHREEQC, which was used for the calculations and inverse modelling in this study.

Moreover, the mineralogical analysis of the mine waste and soil samples was used to determine the phases used in the inverse modelling for magnesite, calcite, gypsum, hematite, quartz, anglesite, halite, hausmannite, muscovite and pyrolusite. We also included halite and gypsum mineral phases that were present in the contaminated soil samples. The MINTEQ thermodynamic database was used for the chemical equilibrium calculations. The main reactions are shown in Table 8. Table 9 shows the main chemical composition of the input and output waters in the simulations.

The results show that the mobilization of Fe, Mn and Pb in the leaching experiment may be caused by the dissolution of hematite, hausmannite, pyrolusite and anglesite. The models obtained (Table 10) show that the dissolution of gypsum and hematite could explain the increase in sulfate

Table 4 Mineralogy of the soils in Las Herrerías

Mineral phases	Formula
Primary phase	
Barite	$BaSO_4$
Breithauptite	NiSb
Canfieldite	Ag_8SnS_6
Millerite	NiS
Oripment	As_2O_3
Polybasite	$(Ag, Cu)_{16}Sb_2S_{11}$
Proustite	Ag_3AsS_3
Stibnite	Sb_2S_3
Secondary phase (low solubility)	
Cerusite	$PbCO_3$
Gibbsite	$Al(OH)_3$
Mimetesite	$Pb_5(AsO_4)_3Cl$
Zincosite	$ZnSO_4$
Secondary phase (low-solubility sulfate minerals)	
Anglesite	$PbSO_4$
Argentojarosite	$Ag_2Fe_6(SO_4)_4(OH)_{12}$
Arcanite	K_2SO_4
Brochantite	$Cu_4(SO_4)(OH)_6$
Butlerite	$Fe(SO_4)(OH) \cdot 2H_2O$
Caracolite	$Na_3Pb_2(SO_4)_3Cl$
Celestite	$SrSO_4$
Chlorothionite	$K_2Cu(SO_4)Cl_2$
Fleischerite	$Pb_3Ge(SO_4)_2(OH)_6 \cdot 3H_2O$
Fibroferrite	$Fe(SO_4)(OH) \cdot 5H_2O$
Guildite	$CuFe(SO_4)_2(OH) \cdot 4H_2O$
Kalistrontite	$KSr(SO_4)_2$
Langite	$Cu_4(SO_4)(OH)_6 \cdot 2H_2O$
Manganolangbeinite	$K_2Mn_2(SO_4)_3$
Mendozite	$NaAl(SO_4)_2 \cdot 11H_2O$
Pickeringite	$MgAl_2(SO_4)_4 \cdot 22H_2O$
Uklonskovite	$NaMg(SO_4)F \cdot 2\ H_2O$
Wherryite	$Pb_7Cu_2(SO_4)(SiO_4)_2(OH)_2$
Secondary phase (medium/high-solubility sulfate minerals)	
Bianchite	$(Zn, Fe)(SO_4)_4 \cdot 6H_2O$
Bieberite	$CoSO_4 \cdot 7H_2O$
Ferrohexahydrite	$FeSO_4 \cdot 6H_2O$
Gunningite	$(Zn, Mn)(SO_4) \cdot H_2O$
Kieserite	$MgSO_4 \cdot H_2O$
Poitevinite	$(Cu, Fe, Zn)(SO_4) \cdot H_2O$
Szmikite	$MnSO_4 \cdot H_2O$
Szomolnokite	$FeSO_4 \cdot H_2O$
Apjhonite	$MnAl_2(SO_4)_4 \cdot 22H_2O$
Halotrichite	$FeAl_2(SO_4)_4 \cdot 22H_2O$
Blödite	$Na_2Mg(SO_4)_2 \cdot 4H_2O$
Sideronatrite	$Na_2Fe(SO_4)_2(OH) \cdot 3H_2O$

Table 5 Principal hydrogeochemical characteristics of groundwater

Element	P-6	P-3	P-5	P-10	EDWS
K	20.6	25.7	45.6	17.9	–
Ca	620.2	460.3	467.5	457.6	–
Mg	350.3	234.6	234.2	234.1	–
Na	414.2	465.6	453	444.9	200
Cl	529.6	592	531.7	549.4	250
SO_4	1,462.4	1,650	1,330	1,295	250
NO_3	30.7	33.4	208	209	50
HCO_3	327.1	317.2	203.1	317.2	–
Al	31.8	5.9	50.1	44.1	200
As	<10	<10	<10	<10	10
Ba	15.4	17.3	17.7	16.6	–
B	1,430	730	740	710	1,000
Cd	<1	<1	<1	<1	5
Cr	<25	<25	<25	<25	50
Cu	<10	<10	<10	<10	2,000
Fe	39.7	204	181.2	23.2	200
Mn	3.3	4.0	7.0	31.6	50
Ni	<20	<20	<20	<20	20
Pb	1.8	1.8	2.5	1.2	10
Sb	<1	<1	<1	<1	5
Se	<50	<50	<50	<50	10
Si	12.1	10.5	10.8	10.7	–
Sr	12.3	8.9	8.7	8.54	–
Zn	20.2	14.2	11.4	12.5	–
EC	6.62	4.4	4.2	4.1	–
PH	8.13	6.75	6.79	7.27	–

Values are in μg L^{-1}, except for K to HCO_3, Si and Sr in mg L^{-1}

EC electrical conductivity in mS cm^{-1}, *EDWS* European drinking water standards

and Fe, while the dissolution of hausmannite and pyrolusite could cause the mobilization of Mn in the lixiviates. In addition, the dissolution of anglesite could increase the sulfate concentration and mobilize the lead in the eluates. Significant amounts of Al were also obtained from the lixiviation tests, which reached 1.57, 0.31 and 5.18 mg L^{-1} in the samples HE1, HE2 and HE3, respectively. These high aluminium concentrations may be due to the weathering of the aluminosilicate minerals, such as muscovite, anorthite or phillipsite (Table 3), or the dissolution of the secondary minerals detected (gibbsite, apjhonite and halotrichite) (Table 4). In fact, under the pH conditions of the leaching tests (8.1–8.3), the aluminium may be solubilized, although the colloidal mobilization could be an important transportation mechanism (Lottermoser 2003). Other lixiviation tests suggest that aluminium concentrations from mine

Table 6 Results of the leaching tests, cations and trace elements

Element:	Na	Mg	Si	K	Ca	Al	Sb	Eu	Mn	Fe	Ni	Cu	Zn	Ba	As	Pb	Sr	Ag	Cd
HE1-1A	>350	73.8	10	55.6	156	1,570	13.9	8.52	1,650	900	33	73	221	26	1.9	1590	1,570	<2	0.6
HE1-2A	>350	> 200	8	171	> 200	420	17.1	2.13	377	300	143	33	66	16	<0.3	401	>2,000	<2	0.3
HE1-3A	>350	108	10	83.5	> 200	1,540	22.6	8.8	1,600	1,100	49	52	205	17	0.4	1,430	1,920	2	0.4
HE1-4A	>350	61.7	8	43	155	100	7.3	0.69	89	<100	22	5	16	19	2.1	96.9	1,290	<2	<0.1
HE1-5A	318	49.9	8	34.6	137	50	6.4	0.35	44	<100	12	3	9	22	2.3	47.6	1,180	<2	<0.1
HE1-6A	247	41.2	8	26.7	121	50	5.5	0.24	30	<100	11	2	7	25	2.2	30.8	964	<2	<0.1
HE1-7A	186	32	8	19.7	99	50	5.0	0.32	34	<100	4	< 2	9	27	2.1	38.8	783	<2	<0.1
HE1-8A	130	24.3	9	12.9	83	40	3.8	0.17	16	<100	< 3	15	5	41	1.8	17.0	578	<2	<0.1
HE1-9A	120	21.2	8	12.2	79	30	3.1	0.12	12	<100	< 3	< 2	< 5	40	1.6	13.6	523	<2	<0.1
HE1-10A	132	24.2	8	13.3	80	20	3.2	0.03	4	<100	< 3	< 2	< 5	53	1.3	4.1	572	<2	<0.1
HE1-11A	121	22.6	8	13.2	81	50	3.6	0.34	32	<100	< 3	< 2	11	36	1.7	34.2	580	<2	<0.1
HE1-12A	112	21.5	8	12.2	83	40	3.8	0.25	22	<100	< 3	< 2	6	37	1.7	47.6	615	<2	<0.1
HE2-1A	>350	98.9	13	124	> 200	310	19.5	5.6	161	<100	14	28	93	22	1.6	188	1,810	11	0.4
HE2-2A	344	77.2	13	96.8	> 200	40	16.3	0.32	12	<100	14	9	20	15	0.8	13.3	1,590	8	0.2
HE2-3A	198	48.2	12	58.8	> 200	40	13.8	0.21	7	<100	4	6	11	18	0.8	10.7	1,350	3	0.1
HE2-4A	129	32.7	12	42.2	193	30	12.4	0.11	5	<100	< 3	5	11	21	0.9	6.3	1,220	<2	<0.1
HE2-5A	73.5	21.8	11	26.2	140	20	11.7	0.09	4	<100	< 3	4	13	27	1	5.1	140	<2	<0.1
HE2-6A	53.6	15.7	11	18.7	117	20	11.2	0.09	3	<100	< 3	3	6	34	0.8	4.3	1,060	<2	<0.1
HE2-7A	33.9	10.4	10	11.5	82	20	10.1	0.04	2	<100	< 3	3	6	56	0.5	3.5	963	<2	<0.1
HE2-8A	27.4	8.6	10	8.8	72	20	9.3	0.03	1	<100	< 3	< 2	< 5	81	0.7	3.0	910	<2	<0.1
HE2-9A	21.6	7.2	10	5.9	53	20	8.6	0.03	2	<100	< 3	< 2	< 5	136	0.7	3.1	841	<2	<0.1
HE2-10A	20.3	6.7	10	4.6	47	20	7.4	0.06	2	<100	< 3	< 2	14	198	0.8	4.2	792	<2	<0.1
HE2-11A	17.9	6.0	9	3.8	44	20	6.5	0.03	< 1	<100	< 3	< 2	< 5	250	< 0.3	2.3	695	<2	<0.1
HE2-12A	17.4	6.0	10	3.5	44	30	5.9	0.02	< 1	<100	< 3	< 2	7	261	0.5	2.3	636	<2	<0.1
HE2-13A	17.7	5.9	10	3.2	47	20	5.6	0.05	1	<100	< 3	< 2	< 5	332	0.6	3.2	624	<2	<0.1
HE3-1A	85.2	31.9	15	39.9	> 200	5,180	0.6	4.97	4,280	1,800	19	33	510	38	<0.3	651	1,690	22	3.4
HE3-2A	55.5	24.2	13	26.6	184	3,650	0.9	3.31	3,150	2,200	14	19	309	39	<0.3	487	1,300	24	2.2
HE3-3A	44.5	18.6	12	19.2	138	2,640	3.5	1.92	2,330	2,700	8	12	226	56	<0.3	339	986	18	1.1
HE3-4A	39.7	15.2	10	15.1	1,160	1,380	14.4	1.14	1,450	1,300	4	7	92	53	<0.3	213	844	8	0.6
HE3-5A	46.3	17.2	9	19.1	118	810	3.0	0.73	1,040	900	< 3	4	69	46	<0.3	143	919	5	0.4
HE3-6A	57.4	20.4	9	22.4	119	550	3.3	0.37	766	700	< 3	3	48	48	<0.3	89.5	966	2	0.3
HE3-7A	53.8	18.7	9	19.8	110	430	3.1	0.27	654	500	< 3	2	28	47	<0.3	69.6	907	<2	0.2
HE3-8A	48.6	17.2	9	17.3	100	300	2.9	0.25	515	400	< 3	2	110	53	<0.3	59.6	854	<2	0.2
HE3-9A	42.1	14.9	8	14.5	88	120	1.9	0.08	134	<100	< 3	< 2	9	65	<0.3	15.8	678	<2	<0.1
HE3-10A	31.3	11.3	8	10.9	75	60	1.7	0.04	82	<100	< 3	< 2	8	73	0.6	10.7	642	<2	<0.1
HE3-11A	28.3	10.4	8	9.8	72	90	1.8	0.07	152	<100	< 3	< 2	9	75	0.8	17.3	622	<2	<0.1
HE3-12A	27.4	10.7	9	9.1	72	410	2.4	0.33	652	400	< 3	2	30	76	0.4	85.4	625	2	0.2

Values are in μg L^{-1}, except for Na to Ca (mg L^{-1})

tailings are limited by gibbsite solubility and only minor amounts of aluminium may be expected to be derived from the dissolution of muscovite (Jurjovec et al. 2002). The dissolution of carbonates, such as calcite, magnesite and ankerite may lead to the consumption of hydrogen ions, which maintain the pH of leachates over neutrality.

Chloride concentrations in the column experiments (Table 7) showed the elution of decreasing Cl^- concentrations in the three experiments, which may indicate the dissolution of halite or halide compounds, as suggested by the modelling (Table 10). Sulfate, the predominant anion, shows a maximum dissolved concentration of 1,180 mg L^{-1} in the sample HE2 (Table 7), which mainly consists of sulfate minerals. The sulfate concentrations remain lower only after the first 15 pore volumes, indicating the possible dissolution of gypsum and other sulfate-mineral phases during the lixiviation experiments. The results of the inverse modelling thus indicate that gypsum dissolution

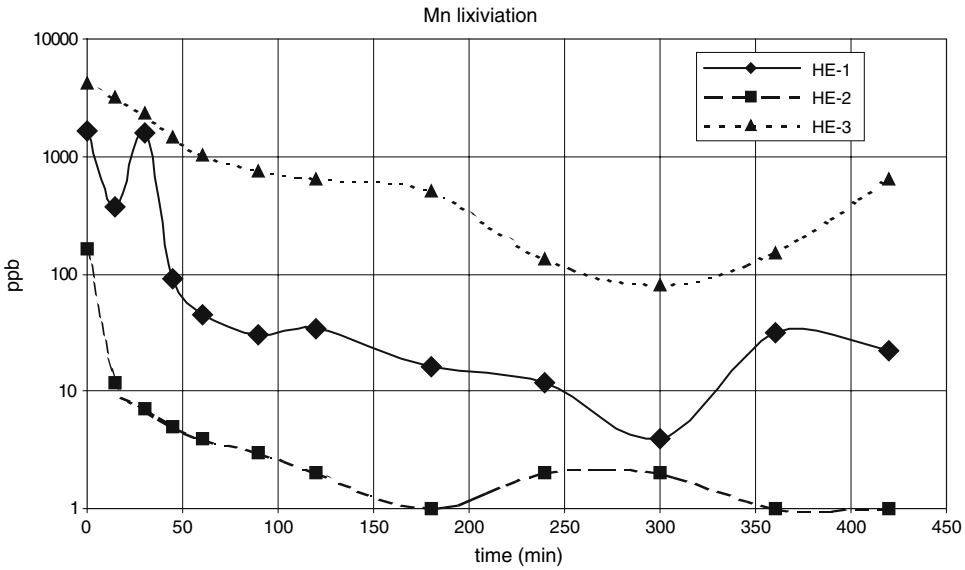

Fig. 5 Change of Mn content in time, measured in efluent solution of column leaching tests. *HE1* old mine waste, *HE2* barite spoils and *HE3* present mining wastes

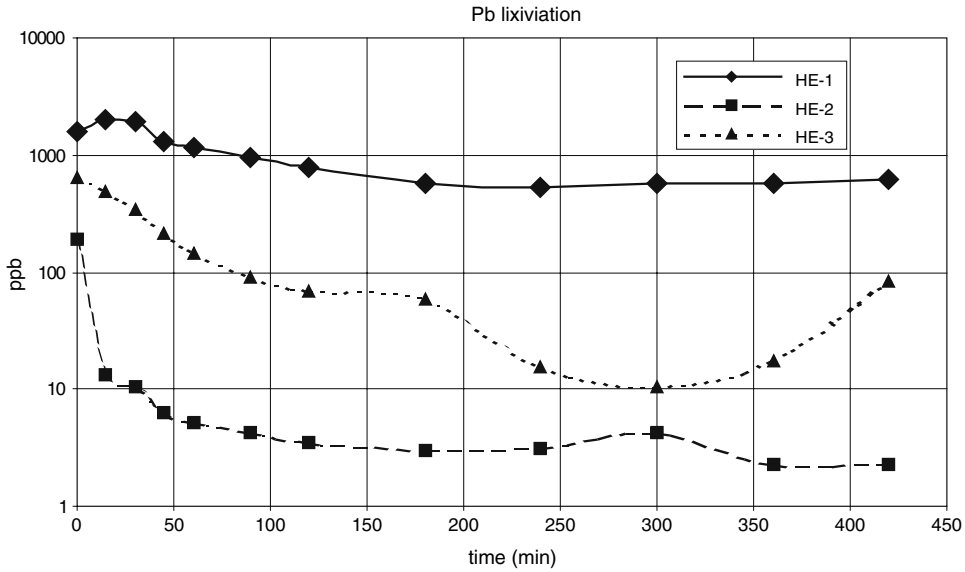

Fig. 6 Change of Pb content in time, measured in efluent solution of column leaching tests. *HE1* old mine waste, *HE2* barite spoils and *HE3* present mining wastes

may control the sulfate concentrations in the leachates (Table 10).

Solid-phase controls on the mobility of main contaminants

Silver

The silver concentration in the lixiviates may be caused by the presence of chlorargyrite, kongsbergite and argentojarosite in the mine waste and soil samples. The pH–Eh silver diagram shown in Fig. 8 was plotted using the MEDUSA hydrogeochemical code (Puigdomenech 2004) and suggests that metallic silver and AgCl limit the solubility of the element in the pH–Eh conditions of the column experiments. In natural water, the concentration varies between 0.3–10 μg L^{-1} (Hem 1989), while in the lixiviates, it ranges between <2 and 24 μg L^{-1}.

If we consider that Ag forms even stronger complexes with Cl and "soft" halogens such as Br and I (Langmuir et al. 2005) and high concentrations of these two elements are detected, it is reasonable to assume that they are responsible for the high concentrations of Ag in the eluates.

Europium

The most stable oxidation state for lanthanide elements, including europium, is +3. The Eh–pH diagram in Fig. 9 therefore shows that $Eu(OH)_3$ is probably the solid phase which controls the solubility of Eu in the pH–Eh conditions

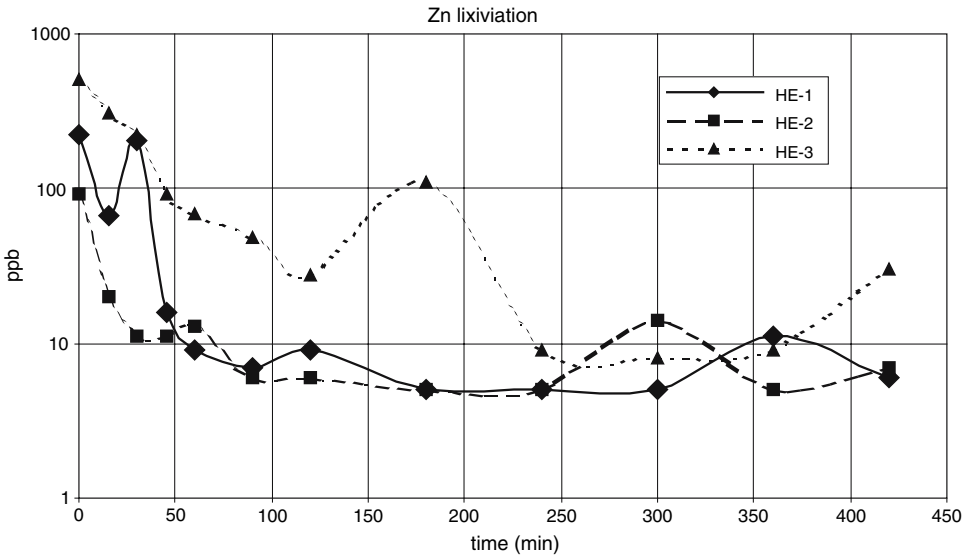

Fig. 7 Change of Zn content in time, measured in efluent solution of column leaching tests. *HE1* old mine waste, *HE2* barite spoils and *HE3* present mining wastes

of the experiments. Krupca and Senne (2002) stated that $Eu(OH)_3$ was the only likely solubility control for Eu under alkaline conditions.

In the absence of dissolved carbonate, the solubility of $Eu(OH)_3$ is exceeded at 10^{-8} mol L^{-1} total dissolved Eu (Krupca and Senne 2002). The Eu detected in the lixiviates was thus oversaturated compared to the solid phase and should indicate the mobilization of Eu in carbonate or other complexes.

Manganese

The high concentrations of Mn in the lixiviates (1.65 mg L^{-1} in HE1 and 4.28 mg L^{-1} in HE3) are apparently caused by the dissolution of hausmannite and possibly pyrolusite (detected only in hand samples), which was detected in the mine wastes.

Figure 10 shows the pH–Eh diagram for the system Mn–O_2–Cl–S–H_2O and indicates a correlation between the stability region for Mn^{2+} and the pH–Eh conditions in the column experiments, which may explain the high concentration of dissolved Mn.

Iron, lead and zinc

The dissolution of hematite and hydrohematite could be the source of Fe in the lixiviates, although the presence of secondary sulfate phases, such as szomolnokite, argentojarosite, bianchite and halotrichite and their dissolution in warm periods may also account for the concentrations of dissolved Fe in the lixiviates (1.1 mg L^{-1} in HE1 and 2.7 mg L^{-1} in HE3). These concentrations are similar to the low Fe concentrations of mildly acidic leachates of cemented tailings in Pb–Zn impoundments (Romero et al. 2007).

The oxidation of galena is often the primary source of dissolved lead in tailings and mine-waste leachates. Geochemical modelling indicates that the presence of dissolved Pb (1.5 mg L^{-1} in HE1) may be caused by the dissolution of anglesite. Mineralogical determinations show that anglesite, macedonite, caracolite, fleischerite and wherryite are present in the mine soils. Anglesite and plumbojarosite are therefore weakly soluble if the pH rises (Romero et al. 2007).

Zinc can be released into leachates by means of the oxidation and dissolution of sphalerite. This mineral phase is not detected in the mineralogical study, although it was recorded in a previous analysis of the Las Herrerias mineral deposit (Martínez et al. 1992). In fact, the presence of secondary phases, such as bianchite, gunningite and poitevinite may indicate oxidation of sphalerite and the subsequent formation of these sulfate minerals which in dissolved form could explain the levels of Zn detected in the lixiviates (0.22 mg L^{-1} in HE1 and 0.51 mg L^{-1} in HE3).

Conclusions

Barite-rich ore stockpiles and mining waste dumps from the Las Herrerías mine are exposed to weathering processes that may lead to the mobilization of Ag, Al, Ba, Cu, Cd, Eu, Fe, Mn, Ni, Sb, Pb and Zn into the local drainage system, surrounding aquifers and fluvial sediments of the Almanzora river basin.

The mine wastes from this area show high concentrations of Ag, As, Ba, Fe, Hg, Sb, Eu, Pb, Zn and Mn. The mineralogies of the wastes are very diverse and consist of dominant species and minor phases. The most abundant primary mineral phases are hematite, hydrohematite, barite, quartz, muscovite, anorthite, calcite and phillipsite. The minor phase minerals are primary minerals, such as ankerite, cinnabar, digenite, magnesite, stannite, siderite

Table 7 Results of the leaching tests. Main anions and parameters measured "in situ"

Element	Time (min)	pH	Eh (mV)	EC (mS cm^{-1})	O_2 (mg L^{-1})	Cl (mg L^{-1})	NO_2 (as N) (mg L^{-1})	NO_3 (as N) (mg L^{-1})	PO_4 (as P) (mg L^{-1})	SO_4 (mg L^{-1})	Alk. (mg L^{-1} CaCO3)
HE1-1A	0	8.2	20	4.5	8.3	500	<0.1	4.3	<0.3	565	106
HE1-2A	15	8.16	71	3.9	8.0	919	<0.2	7.7	<0.4	942	103
HE1-3A	30	8.18	94	3.9	7.8	860	<0.2	7.2	<0.4	927	103
HE1-4A	45	8.2	110	2.8	7.1	453	<0.1	3.9	<0.2	529	104
HE1-5A	60	8.2	121	2.5	6.9	379	<0.10	3.3	<0.2	449	103
HE1-6A	90	8.26	120	1.9	6.8	288	<0.07	2.5	<0.1	340	104
HE1-7A	120	8.23	131	1.2	6.9	205	<0.05	1.9	<0.1	248	106
HE1-8A	180	8.27	131	1.1	6.8	145	<0.04	1.4	<0.08	182	107
HE1-9A	240	8.21	194	1.0	6.9	132	<0.04	1.3	<0.08	164	108
HE1-10A	300	8.22	161	1.1	7.2	147	<0.03	1.4	<0.07	182	108
HE1-11A	360	8.21	132	1.0	7.1	135	<0.04	1.3	<0.08	172	107
HE1-12A	420	8.24	150	0.9	7.1	120	<0.04	1.2	<0.07	172	106
HE2-1A	0	8.13	148	4.7	7.8	784	<0.2	17	<0.4	1,180	96
HE2-2A	10	8.11	150	2.8	7.3	387	<0.1	9.5	<0.3	798	99
HE2-3A	20	8.06	155	2.0	7.4	221	<0.08	5.7	<0.2	572	101
HE2-4A	30	8.1	160	1.4	7.5	140	<0.06	3.8	<0.1	428	102
HE2-5A	45	8.14	152	1.0	7.3	19.5	<0.01	0.54	<0.02	71.8	102
HE2-6A	60	8.21	163	0.7	7.1	53.4	<0.03	1.5	<0.06	211	103
HE2-7A	90	8.23	150	0.5	7.2	34.2	<0.02	0.97	<0.05	129	106
HE2-8A	120	8.19	168	0.4	7.6	26.7	<0.02	0.76	<0.03	85.4	108
HE2-9A	180	8.3	155	0.3	7.4	20.4	<0.01	0.59	<0.03	42.2	110
HE2-10A	240	8.3	145	0.2	7.6	17.9	<0.01	0.52	<0.03	27.3	110
HE2-11A	300	8.3	140	0.2	7.1	16.5	<0.01	0.48	<0.02	21.8	110
HE2-12A	360	8.32	145	0.2	7.4	15.7	<0.01	0.45	<0.02	19.1	109
HE2-13A	420	8.25	142	0.2	7.4	15.2	<0.01	0.45	<0.02	17.4	111
HE3-1A	0	8.23	174	0.8	7.2	90.9	<0.04	3	<0.08	257	100
HE3-2A	15	8.16	173	0.8	7.1	60.8	<0.03	2	<0.06	208	102
HE3-3A	30	8.16	173	0.8	7.0	56.2	<0.03	1.9	<0.06	198	101
HE3-4A	45	8.13	167	0.8	7.2	50.5	<0.03	1.7	<0.06	183	103
HE3-5A	60	8.11	167	0.9	7.2	85.2	<0.03	3	<0.06	218	101
HE3-6A	90	8.15	161	0.9	7.1	77.7	<0.03	2.8	<0.07	203	102
HE3-7A	120	8.16	156	0.8	7.4	67.4	<0.03	2.4	<0.06	179	101
HE3-8A	180	8.2	154	0.8	7.2	61.3	<0.03	2.1	<0.06	163	102
HE3-9A	240	8.22	151	0.6	7.2	52.9	<0.03	1.8	<0.05	142	103
HE3-10A	300	8.24	148	0.5	7.1	42.8	<0.02	1.4	<0.05	127	103
HE3-11A	360	8.23	146	0.5	7.3	37.5	<0.02	1.3	<0.04	114	103
HE3-12A	420	8.24	145	0.4	7.2	35.8	<0.02	1.2	<0.04	104	105

and jamesonite; and secondary minerals such as glauberite, szomolnokite, thenardite and uklonskovite.

The soil samples show high concentrations of Ag (mean 21.6 mg kg^{-1}), Ba (mean 2.5%), Fe (mean 114,000 mg kg^{-1}), Sb (mean 342.5 mg kg^{-1}), Pb (mean 1,229.8 mg kg^{-1}), Zn (mean 493 mg kg^{-1}), Mn (mean 4,321.1 mg kg^{-1}), Cd (mean 1.2 mg kg^{-1}) and Eu (mean 4.0 mg kg^{-1}).

Column experiments used to simulate the mobilization of heavy metals and metalloids reveal solubilization of Ag, Al, Ba, Cu, Cd, Eu, Fe, Mn, Ni, Sb, Pb and Zn. Inverse modelling applied to the mass transfer between the demineralized input water and the first lixiviate of the HE1 sample (old mine wastes) shows that the mobilization of Fe, Mn and Pb in the leaching experiment is largely caused by the dissolution of hematite, hausmannite, pyrolusite and anglesite.

The mobility of silver may be due to the presence of kongsbergite and chlorargyrite in the wastes and the MEDUSA hydrogeochemical code suggests that metallic

Table 8 Mineral phases used in the inverse modelling

Phases	Reaction	Log K (MINTEQ)
Calcite	$CaCO_3 = Ca^{2+} + CO_3^{2-}$	–8.47
Magnesite	$Mg(CO_3) = Mg^{2+}\ CO_3^{2-}$	–8.029
Gypsum	$Ca(SO_4)\cdot 2H_2O = Ca^{2+} + SO_4^{2-} + 2H_2O$	–4.848
Quartz	$SiO_2 + 2H_2O = 4H_4SiO_4$	–4.006
Halite	$NaCl = Na^+ + Cl^-$	1.582
Hematite	$Fe_2O_3 + 6H^+ = 2Fe^{3+} + 3H_2O$	–4.008
Muscovite	$KAl_3Si_3O_{10}(OH)_2 + 10H^+ = K^+ + 3Al^{3+} + 3H_4SiO_4$	12.99
Anglesite	$PbSO_4 = Pb^{2+} + SO_4^{2-}$	–7.79
Pyrolusite	$MnO_2 + 4H^+ + e^- = Mn^{3+} + 2H_2O$	15.861
Hausmannite	$Mn_3O_4 + 8H^+ + 2e^- = 3Mn^{2+} + 4H_2O$	61.54

Table 9 Input data and output concentrations used in the inverse modelling

Parameter	Input[a]	Output[b]
pH	7.0	8.2
Eh (mV)	261	20
Ca (mg L^{-1})	38.2	156
Mg (mg L^{-1})	3.36	73.8
Na (mg L^{-1})	13.0	350.0
K (mg L^{-1})	1.12	55.6
SO_4 (mg L^{-1})	13.2	565
HCO_3 (mg L^{-1})	110.0	106
Cl (mg L^{-1})	13.4	500
O2 (mg L^{-1})	8.59	8.3
Fe (μg L^{-1})	1	900
Mn (μg L^{-1})	0.1	1,650
Pb (μg L^{-1})	0.37	1,590
Si (mg L^{-1})	9.5	10.0

[a] Demineralized water

[b] Lixiviate HE1-1

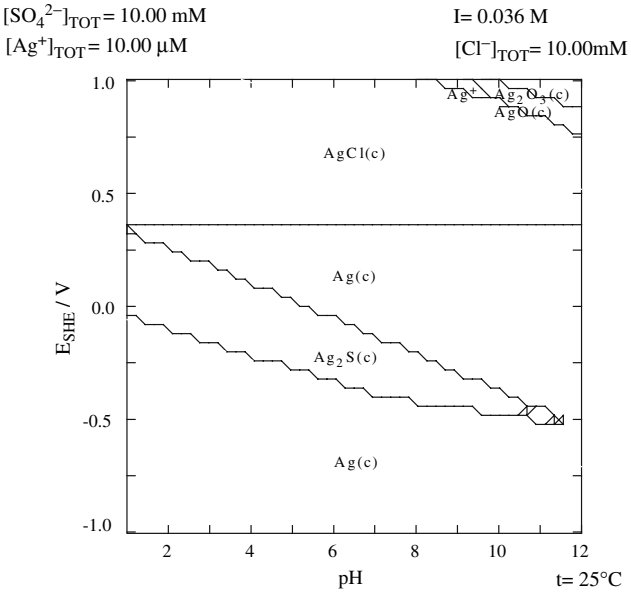

Fig. 8 Eh–pH diagram for the Ag–O_2–Cl–S–H_2O system. *c* Solid phase, E_{SHE}/V Eh (v)

silver and AgCl may limit the solubility of the element in the pH–Eh conditions of the column experiments. This hypothesis is further corroborated by that fact that Ag can form stronger complexes with Cl and "soft" halogens such as Br and I.

The mobility of Eu is apparently dependent on $Eu(OH)_3$, which controls the solubility of Eu in the pH–Eh conditions of the experiments. However, in the absence of dissolved carbonate, the solubility of $Eu(OH)_3$ is exceeded at 10^{-8} mol L^{-1} total dissolved Eu. As a consequence, the Eu detected in the lixiviates was oversaturated with regard to this solid phase and should indicate mobilization of Eu in carbonate or other complexes.

The mobility of Fe seems to be largely caused by the dissolution of hematite, which occurs in carbonate controlled systems (pH > 7.0) through CO_3 complexation. However, due to the presence of marly clays in the "host-rocks" and a possible thick non-saturated zone in the

Table 10 Models and molar transfers calculated by PHREEQC

Phases	M1	M2	M3	M4	M5	M6
Magnesite	2.93×10^{-3}	2.93×10^{-3}	2.93×10^{-3}	2.93×10^{-3}	2.93×10^{-3}	$2.93\cdot 10^{-3}$
Calcite	-2.69×10^{-3}	-2.69×10^{-3}	-2.69×10^{-3}	-2.69×10^{-3}	-2.69×10^{-3}	-2.69×10^{-3}
Gypsum	5.83×10^{-3}	5.83×10^{-3}	5.83×10^{-3}	5.83×10^{-3}	5.83×10^{-3}	5.83×10^{-3}
Hematite	8.06×10^{-6}	8.06×10^{-6}	8.06×10^{-6}	8.06×10^{-6}	8.06×10^{-6}	8.06×10^{-6}
Quartz	5.38×10^{-6}	–	5.38×10^{-6}	–	5.38×10^{-6}	–
Anglesite	9.65×10^{-7}	9.65×10^{-7}	9.65×10^{-7}	9.65×10^{-7}	9.65×10^{-7}	9.65×10^{-7}
Halite	1.36×10^{-2}	1.36×10^{-2}	1.36×10^{-2}	1.36×10^{-2}	1.36×10^{-2}	1.36×10^{-2}
Hausmannite	2.75×10^{-5}	–	1.00×10^{-5}	1.00×10^{-5}	–	2.75×10^{-5}
Pyrolusite	-5.25×10^{-5}	3.03×10^{-5}	–	–	3.00×10^{-5}	-5.25×10^{-5}

Negative values indicate precipitation and positive values indicate dissolution

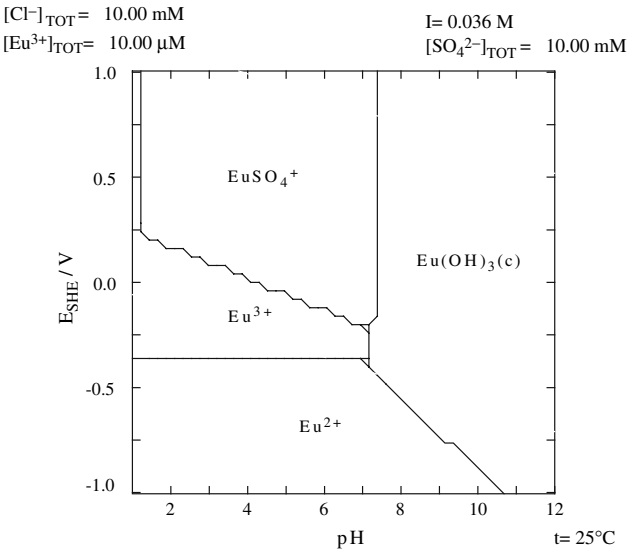

Fig. 9 Eh–pH diagram for the Eu–O_2–Cl–S–H_2O system. **c** Solid phase, E_{SHE}/V Eh (v)

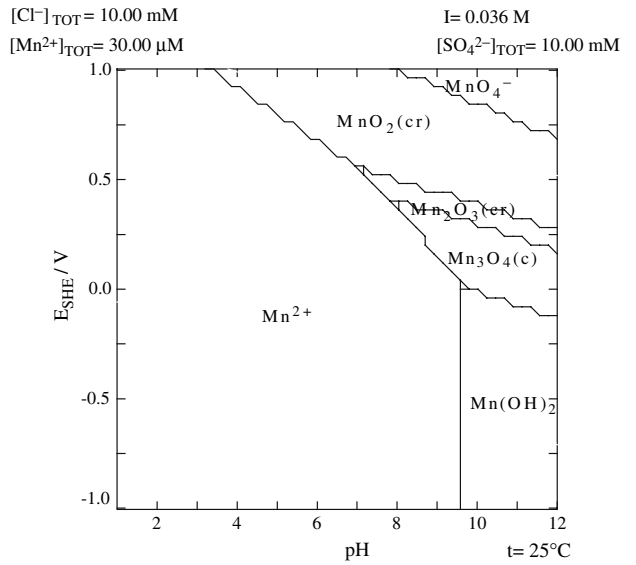

Fig. 10 Eh–pH diagram for the Mn–O_2–Cl–S–H_2O system. *c* Solid phase, E_{SHE}/V Eh (v)

nearby aquifers, the groundwater shows no clear evidence of mining contamination.

Acknowledgments This study was supported by the Spanish Ministry of Science and Technology (projects REN2003-09247-C04-03 and ENE2006-13267-C05-03) in collaboration with CIEMAT (the Centre for Energy, Environmental and Technological Research). We are grateful to the staff of the Department of Fluid Mechanics (UPC) for carrying out the leaching experiments. The authors are grateful to the anonymous reviewers for their constructive comments.

References

Al TA, Martin CJ, Blowes DW (2000) Carbonate-mineral/water interactions in sulfide-rich mine tailings. Geochim Cosmochim Acta 64:3933–3948

Armienta MA, Villaseñor G, Rodríguez R, Ongley LK, Mango H (2001) The role of arsenic-bearing rocks in groundwater pollution at Zimapán Valley, México. Environ Geol 40:571–581

Ashley PM, Lottermoser BG, Collins AJ, Grant CD (2004) Environmental geochemistry of the derelict Webbs Consols mine, New South Wales, Australia. Environ Geol 46:591–604

Blowes DW, Jambor JL (1990) The pore water geochemistry and the mineralogy of the vadose zone of sulfide tailings, Waite Amulet, Quebec Canada. Appl Geochem 5:327–346

Blowes DW, Ptacek CJ (1994) Acid-neutralization mechanisms in inactive mine tailings. In: Jambor JL, Blowes DW (ed) The environmental geochemistry of sulfide-mine wastes. Mineralogical Association of Canada, Short course handbook 22:271–292

Blowes DW, Ptacek CJ, Jurjovec J (2003) Mill tailings: hydrogeology and geochemistry. In: Jambor JL, Blowes DW, Ritchie AIM (ed) Environmental aspects of mine wastes. Mineralogical Association of Canada, Short course series 31:95–116

Blowes DW, Ptacek CJ, Jambor JL, Weisener CG (2004) The geochemistry of acid mine drainage. In: Holland H, Turekian K (ed) Treatise on geochemistry. Environ Geochem 9:149–204

Buckby RA, Otton JK, Johnson CA (2003) Fe-sulphate-rich evaporite mineral precipitates from the Río Tinto, southwest Spain. Mineral Mag 67:263–278

Booth-Rea G, Azañón JM, García-Dueñas V, Augier R (2003) Uppermost tortonian to quaternary depocentre migration related with segmentation of the strike-slip Palomares fault-zone, Vera Basin (SE Spain). C R Geosci 335:751–761

Dold B, Fontboté L (2001) Element cycling and secondary mineralogy in porphyry copper tailings as a function of climate, primary mineralogy and mineral processing. J Geochem Explor 74:3–55

Dold B, Fontboté L (2002) A mineralogical and geochemical study of element mobility in sulfide mine tailings of Fe oxide Cu–Au deposits from the Punta del Cobre belt, nothern Chile. Chem Geol 189:135–163

EPA (1996) Managing environmental problems at inactive and abandoned metal mine sites. EPA/625/R-95/007

Eary LE, Runnels DD, Esposito KJ (2003) Geochemical controls on groundwater composition at the Cripple Creek Mining District, Colorado. Appl Geochem 18:1–24

Harris DL, Lottermoser BG, Duchesne J (2003) Ephemeral acid mine drainage at the Montalbion silver mine, north Queensland. Aust J Earth Sci 50:797–809

Hem JD (1989) Study and interpretation of the chemical characteristics of natural water. Water-supply paper 2254. US Geological Survey, Reston

Herbert RB (1996) Metal retention by iron oxide precipitation from acidic ground water in Dalarna, Sweden. Appl Geochem 11:229–235

Jambor JL, Nordstrom DK, Alpers CN (2000) Metal-sulfate salts from sulfide mineral oxidation. In: Alpers CN, Jambor JL, Nordstrom DK (ed) Sulfate minerals—crystallography, geochemistry, and environmental significance. Mineral Soc Am, Rev Mineral Geochem 40:303–350

Jurjovec J, Ptacek CJ, Blowes DW (2002) Acid neutralization mechanisms and metal release in mine tailings: a laboratory column experiment. Geochim Cosmochim Acta 66:1511–1523

Kelley KD, Seal RR, Schmidt JM, Hoover DB, Klein DP (1996) Sedimentary exhalative Zn–Pb–Ag deposits (model 31 a). Open-file report 95–831. US Geological Survey, Reston

Krupca KM, Senne RJ (2002) Geochemical factors affecting the behaviour of antimony, cobalt, europium, technetium and uranium in Vadose sediments. Pacific Northwest National Laboratory. PNNL-14126

Langmuir D, Chrostowski P, Vigneault B, Chaney R (2005) Issue paper on the environmental chemistry of metals. Risk Assessment Forum, US EPA, Contract 68-C-02–060

López J, Martínez J, Lunar R, López García JA (1993) El rombohorst mineralizado de Las Herrerías: un caso de "doming" e hidrotermalismo submarino mioceno en el SE ibérico. Estudios Geológicos 49:13–19

Lottermoser BG (2003) Mine wastes: characterization, treatment and environmental impacts. Springer, Berlin, pp 277

McGregor RG, Blowes DW, Jambor JL, Robertson WD (1998) The solid-phase controls on the mobility of heavy metals at the Copper Cliff tailings area, Sudbury, Ontario, Canada. J Contam Hydrol 33:247–271

Mahlknecht J, Schneider JF, Merkel BJ, Navarro de León I, Bernasconi SM (2004) Groundwater recharge in a sedimentary basin in semi-arid México. Hydrogeol J 12:511–530

Martínez J, García J, López Ruiz J, Reynolds GA (1992) Discovery of fossil fumaroles in Spain. Econ Geol 87:444–447

Navarro A, Martínez J, Font X, Viladevall M (2000) Modelling of modern mercury vapor transport in an ancient hydrothermal system: environmental and geochemical implications. Appl Geochem 15:281–294

Navarro A, Collado D, Carbonell M, Sánchez JA (2004) Impact of mining activities in a semi-arid environment: Sierra Almagrera district, SE Spain. Environ Geochem Health 26:383–393

Navarro A, Biester H, Mendoza JL, Cardellach E (2006) Mercury speciation and mobilization in contaminated soils of the Valle del Azogue Hg mine (SE, Spain). Environ Geol 49:1089–1101

Parkhurst DL, Appelo CAJ (1999) User's guide to PHREEQC (version 2)—a computer program for speciation, batch-reaction, one-dimensional transport, and inverse geochemical calculations. Water-resources investigations report 99–4259. US Geological Survey, Reston, pp 326

Ptacek CJ, Blowes WD (2003) Geochemistry of concentrated waters at miner-waste sites. In: Jambor JL, Blowes DW, Ritchie AIM (eds) Environmental aspects of mine wastes. Mineralogical Association of Canada, Short course series 31:239–252

Puigdomenech I (2004) Make equilibrium using sophisticated algorithms (MEDUSA) program. Inorganic Chemistry Department. Royal Institute of Technology, Stockholm. http://web.telia.com/

Ribet I, Ptacek CJ, Blowes DW, Jambor JL (1995) The potential for metal release by reductive dissolution of weathered mine tailings. J Contam Hydrol 17:239–273

Robles-Arenas VM, Rodríguez R, García C, Manteca JI, Candela L (2006) Sulphide-mining impacts in the physical environment: Sierra de Cartagena-La Unión (SE Spain) case study. Environ Geol 51:47–64

Romero FM, Armienta MA, Villaseñor G, González JL (2006) Mineralogical constraints on the mobility of arsenic in tailings from Zimapán, Hidalgo, Mexico. Int J Environ Pollut 26:23–40

Romero FM, Armienta MA, González-Hernández JL (2007) Solid-phase control on the mobility of potentially toxic elements in an abandoned lead/zinc mine tailings impoundment, Taxco, Mexico. Appl Geochem 22:109–127

Rytuba JJ (2003) Mercury from mineral deposits and potential environmental impact. Environ Geol 43:326–338

Schwartz MO (1997) Mercury in zinc deposits: economic geology of a polluting element. Int Geol Rev 39:905–923

Stollenwerk KG (1994) Geochemical interactions between constituents in acidic groundwater and alluvium in an aquifer near Globe, Arizona. Appl Geochem 9:353–369

Wray DS (1998) The impact of unconfined mine tailings and anthropogenic pollution on a semi-arid environment: an initial study of the Rodalquilar mining district, southeast Spain. Environ Geochem Health 20:29–38